Analysis of time-multiplexed optical line-by-line pulse shaping: application for radio-frequency and microwave photonics

Chen-Bin Huang[1,*], Andrew M. Weiner[2]

[1]*Institute of Photonics Technologies, National Tsing Hua University, 101 Sec. 2, Kuang-Fu Road, Hsinchu, 30013, Taiwan*
[2]*School of Electrical and Computer Engineering, Purdue University, 465 Northwestern Avenue, West Lafayette, IN, 47907, USA*
robin@ee.nthu.edu.tw

Abstract: Time-multiplexed optical line-by-line pulse shaping with specific application to rapid update radio-frequency (RF) waveform generation is modeled. The effects of fundamental pulse shaping parameters on generated RF waveforms are numerically analyzed. Experimental and theoretical results are compared and are in excellent agreement.

OCIS codes: (320.0320) Ultrafast optics; (320.5540) Pulse shaping; (060.5625) Radio frequency photonics; (350.4010) Microwaves.

References and links

1. Z. Jiang, D. S. Seo, D. E. Leaird, and A. M. Weiner, "Spectral line-by-line pulse shaping," Opt. Lett. **30**(12), 1557–1559 (2005).
2. A. M. Weiner, "Femtosecond pulse shaping using spatial light modulators," Rev. Sci. Instrum. **71**(5), 1929–1960 (2000).
3. A. M. Weiner, "Manipulation of ultrashort pulses," in *Ultrafast Optics* (Wiley, 2009), pp. 362–421.
4. J. Ye, and S. T. Cundiff, eds., *Femtosecond Optical Frequency Comb: Principle, Operation, and Applications* (Springer, 2005).
5. Z. Jiang, C.-B. Huang, D. E. Leaird, and A. M. Weiner, "Optical arbitrary waveform processing of more than 100 spectral comb lines," Nat. Photonics **1**(8), 463–467 (2007).
6. Z. Jiang, D. E. Leaird, and A. M. Weiner, "Line-by-line pulse shaping control for optical arbitrary waveform generation," Opt. Express **13**(25), 10431–10439 (2005).
7. V. R. Supradeepa, C.-B. Huang, D. E. Leaird, and A. M. Weiner, "Femtosecond pulse shaping in two dimensions: towards higher complexity optical waveforms," Opt. Express **16**(16), 11878–11887 (2008).
8. N. K. Fontaine, R. P. Scott, J. Cao, A. Karalar, W. Jiang, K. Okamoto, J. P. Heritage, B. H. Kolner, and S. J. B. Yoo, "32 Phase X 32 amplitude optical arbitrary waveform generation," Opt. Lett. **32**(7), 865–867 (2007).
9. N. K. Fontaine, R. P. Scott, C. Yang, D. J. Geisler, J. P. Heritage, K. Okamoto, and S. J. B. Yoo, "Compact 10 GHz loopback arrayed-waveguide grating for high-fidelity optical arbitrary waveform generation," Opt. Lett. **33**(15), 1714–1716 (2008).
10. E. Frumker, E. Tal, Y. Silberberg, and D. Majer, "Femtosecond pulse-shape modulation at nanosecond rates," Opt. Lett. **30**(20), 2796–2798 (2005).
11. T. Yilmaz, C. M. DePriest, T. Turpin, J. H. Abeles, and P. J. Delfyett, "Towards a photonic arbitrary waveform generator using a modelocked external cavity semiconductor laser," IEEE Photon. Technol. Lett. **14**(11), 1608–1610 (2002).
12. M. H. Khan, H. Shen, Y. Xuan, L. Zhao, S. Xiao, D. E. Leaird, A. M. Weiner, and M. Qi, "Ultrabroad-bandwidth arbitrary radiofrequency waveform generation with a silicon photonic chip-based spectral shaper," Nat. Photonics **4**(2), 117–122 (2010).
13. W. Jiang, *et al*., "A monolithic InP-based photonic integrated circuit for optical arbitrary waveform generation," in *Optical Fiber Conference,* Technical Digest (CD) (Optical Society of America, 2008), Paper JThA39.
14. J. T. Willits, A. M. Weiner, and S. T. Cundiff, "Theory of rapid-update line-by-line pulse shaping," Opt. Express **16**(1), 315–327 (2008).
15. C.-B. Huang, D. E. Leaird, and A. M. Weiner, "Time-multiplexed photonically enabled radio-frequency arbitrary waveform generation with 100 ps transitions," Opt. Lett. **32**(22), 3242–3244 (2007).
16. C.-B. Huang, D. E. Leaird, and A. M. Weiner, "Synthesis of millimeter-wave power spectra using time-multiplexed optical pulse shaping," IEEE Photon. Technol. Lett. **21**(18), 1287–1289 (2009).
17. C.-B. Huang, Z. Jiang, D. E. Leaird, and A. M. Weiner, "The impact of optical comb stability on waveforms generated via spectral line-by-line pulse shaping," Opt. Express **14**(26), 13164–13176 (2006).
18. J. Caraquitena, and J. Martí, "Dynamic spectral line-by-line pulse shaping by frequency comb shifting," Opt. Lett. **34**(13), 2084–2086 (2009).

#125479 - $15.00 USD Received 15 Mar 2010; revised 16 Apr 2010; accepted 19 Apr 2010; published 20 Apr 2010

19. J. Capmany, and D. Novak, "Microwave photonics combines two worlds," Nat. Photonics **1**(6), 319–330 (2007).
20. J. Yao, "Microwave photonics," J. Lightwave Technol. **27**(3), 314–335 (2009).
21. D. E. Leaird, Z. Jiang, and A. M. Weiner, "Experimental investigation of security issues in OCDMA: a code-switching scheme," Electron. Lett. **41**(14), 817–819 (2005).
22. R. P. Scott, N. K. Fontaine, C. Yang, D. J. Geisler, K. Okamoto, J. P. Heritage, and S. J. B. Yoo, "Rapid updating of optical arbitrary waveforms via time-domain multiplexing," Opt. Lett. **33**(10), 1068–1070 (2008).
23. H. Murata, A. Morimoto, T. Kobayashi, and S. Yamamoto, "Optical pulse generation by electrooptic-modulation method and its application to integrated ultrashort pulse generators," IEEE J. Sel. Top. Quantum Electron. **6**(6), 1325–1331 (2000).
24. F. J. Harris, "On the use of windows for harmonic analysis with the discrete Fourier transform," Proc. IEEE **66**(1), 51–83 (1978).
25. J. D. McKinney, I. S. Lin, and A. M. Weiner, "Shaping the Power Spectrum of Ultra-Wideband Radio-Frequency Signals," IEEE Trans. Microw. Theory Tech. **54**(12), 4247–4255 (2006).

1. Introduction

Optical line-by-line pulse shaping [1] combines the functionality of an optical pulse shaper [2,3] with the high frequency stability and long term temporal coherence of an optical frequency comb [4]. With the amplitude and phase of each frequency comb line independently controlled, line-by-line shaped waveforms can span the entire time-domain comb repetition period, thus enabling optical arbitrary waveform generation [5–9]. In addition to the pursuit of shaping large number of comb lines so that high time-domain waveform complexities may be achieved, another research target is the realization of optical arbitrary waveforms with fast waveform update rates (e.g., *dynamic* pulse shaping).

In conventional pulse shapers, the waveform update rate is limited by the response time of the spatial light modulator (SLM). The most commonly adopted SLMs are made of liquid crystals, with response time of the orders of tens of milliseconds. Pulse shaping using such SLM devices can be classified as static shaping regime. Intuitively, dynamic pulse shaping can be achieved by simply replacing the liquid crystals in a static shaper with arrays of electro-optic or electro-absorption modulators with much shorter response times [10,11]. Recent efforts in developing pulse shapers based on planar lightwave circuits (PLC) for compactness have been demonstrated in silica based devices [8,9]. Such PLC shapers have great potential for achieving dynamic shaping by implementation onto semiconductor materials [12,13]. However, rapid waveform update poses complications in the electrical control mechanisms; fully dynamic pulse shaping with waveform update as fast as the period of the input frequency comb (the pulse-by-pulse shaping regime) is yet to be demonstrated. Nevertheless, pulse shaper theory extended to include rapid update in the spatial light modulation has been developed, illustrating a fundamental tradeoff between response speed and waveform fidelity [14].

On the other hand, we have proposed a time-multiplexed line-by-line shaping scheme which should be capable of approaching the pulse-by-pulse shaping regime [15,16]. In this scheme, the time-multiplexing occurs through optical frequency switching before the waveform generation process. A related concept in which waveforms are controlled by adjusting the offset frequency of a frequency comb sources has also been proposed [17,18]. Since these schemes result in switching between waveforms of distinct optical frequencies, they are most suitable for microwave photonics [19,20]. Our intent is to generate designed RF waveforms that are made by incoherently time-multiplexing line-by-line shaped optical waveforms. Since these optical waveforms are at distinct optical frequencies with sufficient separation (greater than the detection electrical bandwidth), and since also we are only observing at RF time scales, the optical signals may be taken to add in intensity (incoherent addition). Dynamic switching between microwave pulses with 10 GHz rate [15] and flexible photonic-assisted tailoring of millimeter-wave power spectra [16] have been experimentally demonstrated via this scheme. Rapid switching between shaped optical waveforms has also been reported using multiple pulse shapers, where waveforms are selected after the pulse shaping process [21,22]. The current scheme allows easy rapid waveform switching among various waveforms using a single pulse shaper. In this report, we present detailed numerical analysis of our scheme for rapid switching of radio-frequency waveforms based on time-

#125479 - $15.00 USD Received 15 Mar 2010; revised 16 Apr 2010; accepted 19 Apr 2010; published 20 Apr 2010

multiplexing prior to line-by-line pulse shaping. Deeper understanding of the effects of the system parameters should bring insight on how to optimize agile RF waveform generation.

The rest of this paper is organized as follows: In section 2, the working principle of our time-multiplexed pulse shaping system is described, and the mathematical formulation for modeling the system is presented. In section 3, the effects of system parameters on time-multiplexed waveforms are numerically analyzed. In section 4, we present a comparison of experimental results with the predictions of the numerical model. The results are in excellent agreement both for time-domain RF waveform intensities and frequency-domain RF power spectra.

2. System description

Figure 1(a) shows the schematic of our time-multiplexed line-by-line pulse shaper. It is comprised of three main functional parts: a rapid wavelength switcher, an optical frequency comb generator, and a waveform bank (an optical line-by-line pulse shaper). The rapid wavelength switcher is made up from two or more continuous-wave (CW) lasers. As a proof of concept, in this paper we assume two CW lasers with center wavelengths of λ_a and λ_b, each followed by a LiNbO3 intensity modulator (IM). Programmable data patterns (Q and $\bar{Q}$) from a pattern generator are used to drive the intensity modulator so to provide rapid wavelength switching. The time-multiplexed wavelength outputs are combined via an optical coupler and directed to an optical frequency comb generator [5,23], which is a $LiNbO_3$ phase modulator (PM). The phase modulator is driven by a time-domain sinusoidal signal with frequency f_{rep}, which determines the resulting optical frequency comb line spacing. These phase-modulated CW (PMCW) combs are then manipulated by a spectral line-by-line shaper using a liquid crystal modulator (LCM) to generate user-specified optical waveforms. Detailed descriptions of the reflective line-by-line shaper can be found in Ref [5]. In order to enable rapid waveform updates, different LCM regions may be programmed to generate different waveforms; the LCM acts as a waveform bank. Different regions of the LCM (hence different waveforms) are selected by rapidly changing the corresponding input wavelength. The waveform update transition time can be less than the frequency comb modulation period, which allows to approach the pulse-by-pulse update regime. Experimentally we have demonstrated a less than 100 ps transition time by using 10 GHz comb repetition frequency [15,16]. An optical amplifier is used to compensate the loss of the shaper for optical or electrical waveform measurements via a fast photo-detector.

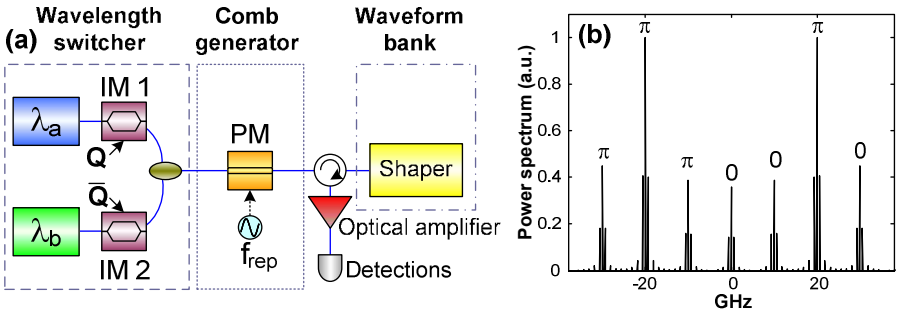

Fig. 1. (a) Schematic of the time-multiplexed shaper. IM: intensity modulator; Q: data pattern; PM: phase modulator; f_{rep}: comb frequency spacing. (b) Calculated PMCW comb for a single CW laser under 16-bit length data pattern. The relative comb spectral phases are labeled.

The proper mathematical description for the waveforms generated by the λ_a and λ_b lasers (with angular frequencies ω_a and ω_b, respectively), can be formulated as

#125479 - $15.00 USD Received 15 Mar 2010; revised 16 Apr 2010; accepted 19 Apr 2010; published 20 Apr 2010

$$e_a(t) = \sqrt{\frac{Q(t)}{2}} \exp\left\{ j[\omega_a t + \Delta_m \cos(\omega_{rep} t)] \right\} \otimes h_a(t) \quad (1a)$$

$$e_b(t) = \sqrt{\frac{\bar{Q}(t)}{2}} \exp\left\{ j[\omega_b t + \Delta_m \cos(\omega_{rep} t)] \right\} \otimes h_b(t) \quad (1b)$$

where $Q(t)$ and $\bar{Q}(t)$ are the intensity responses of the wavelength-switching intensity modulators, Δ_m is the modulation depth of the phase modulator, and $\otimes$ denotes convolution. The output waveform of each laser is convolved with the time-domain shaper impulse response function expressed as [2]:

$$h_i(t) = FT^{-1}\{H_i(\omega)\} = FT^{-1}\left\{ \sqrt{\frac{2}{\pi w_0^2}} \int dx M_i(x) G(x) \right\} \quad (2a)$$

$$G(x) = \exp[-\frac{2(x - \alpha\omega)^2}{w_0^2}] \quad (2b)$$

where FT^{-1} denotes the inverse Fourier-Transform, i = a or b, $H_i(\omega)$ is the effective baseband pulse shaper filter function and $M_i(x)$ is the spatial mask function applied by the LCM to control the comb centered at λ_i respectively. $H_i(\omega)$ is obtained by spatially convolving the mask function against the Gaussian beam intensity $G(x)$. The pulse shaper resolution parameter w_0 denotes the beam waist radius at the LCM plane (half-width at $1/e^2$ of intensity), and α is the spatial dispersion parameter of the pulse shaper in units of cm(rad/s)$^{-1}$. Due to incoherent addition of the optical waveform intensity under the current scheme, the overall time-multiplexed waveform intensity can be expressed as:

$$I(t) = \sum_i |e_i(t)|^2 \quad (3)$$

Intuitively, rapid data modulation of the input laser intensity generates frequency sidebands in the resulting optical frequency comb. This can be made apparent by taking the Fourier transform of Eq. (1): the resulting comb is the original PMCW comb, expressed by the exponential term, convolved with the Fourier spectrum of the data pattern. Figure 1(b) shows one example with a 16-bit length data pattern Q = [1111111100000000] used to modulate a single CW laser before the phase modulator, with each bit duration identical to the comb period $T = 1/f_{rep}$. Here we choose f_{rep} = 10 GHz and $\Delta_m = 0.985V_\pi$, which are in line with our experimental setup [15,16]. Each PMCW comb indeed acquires extra sidebands with frequency spacing of $f_{rep}/16$ beside the original PMCW comb (main lines at integer multiples of 10 GHz. The relative spectral phases of the comb lines directly after the phase modulator (without data modulation) are also labeled [23]). We emphasize here the line-by-line shaping operation is defined with respect to the PMCW comb spacing f_{rep} since we are shaping the pulse waveforms that repeats every period T. The individual frequency sidebands created under the presence of the time-multiplexing need not be resolved.

3. Numerical analysis

Using the basic model formulated in the previous section, the effects of fundamental system parameters on the time-multiplexed waveforms are now analyzed. The main system parameters under investigation include: (1) electrical bandwidth of the data pattern generator and intensity modulator, (2) pulse shaper resolution, (3) finite power extinction ratio in the pulse shaper, and (4) finite extinction ratio in the data modulators. The effects of these four system parameters on waveform fidelity are first examined individually. Our investigation reveals that the two most important parameters are the pulse shaper resolution and intensity

#125479 - $15.00 USD Received 15 Mar 2010; revised 16 Apr 2010; accepted 19 Apr 2010; published 20 Apr 2010

modulator extinction ratio. At the end of this section, we will briefly consider combined effects arising from non-ideal values of multiple system parameters simultaneously.

We note that although a large number of comb lines and a large number of degrees of freedom are involved in typical line-by-line pulse shaping, here we consider very simple shaped waveforms. The intent of this paper is to develop waveform fidelity metrics relevant to time-multiplexed shaper system parameters by using simple, easy-to-understand waveform generation examples. The insights that we gain may also be applied to specific cases of more complex time-multiplexed waveforms as desired.

3.1 Effect of data pattern/intensity modulator bandwidth

The effect of finite electrical bandwidth of the data pattern generator and the intensity modulator leads to finite rise- and fall-times, and is taken into account using a single bandwidth value *BW*. Here a Gaussian filter function of the form $G_{IM}(f) = \exp[-\left(f/BW\right)^2]$ is used to simulate the bandwidth-limited switching pattern. Figure 2(a) shows the data pattern of Q = [1100] assuming *BW* of infinite (solid), 40 GHz (dash) and 12.5 GHz (dot). Each bit occupies 100 ps. Figure 2(b) shows the data (Q, solid) and inverted data ($\overline{Q}$, dot) pattern with *BW* of 12.5 GHz. As we will show in our later analyses, the shaded region, showing rise and fall times of roughly 80 ps, indicates the temporal region with most apparent waveform degradation. This transient duration eventually sets the upper limit on how fast the waveforms can be switched. Therefore pattern generator as well as intensity modulator with electrical bandwidths many times larger (for example, a *BW* value of 40 GHz for f_{rep} = 10 GHz) than the comb modulation frequency would be required to get fully into the pulse-by-pulse update regime. Unless otherwise noted, *BW* of 12.5 GHz is assumed in the following numerical analysis, to conform to our current experimental configurations.

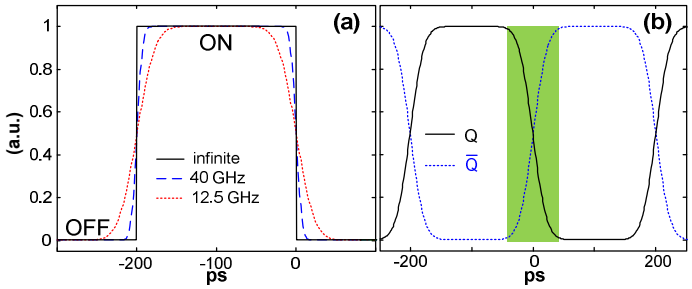

Fig. 2. (a) Data pattern Q = [1100] with BW values of infinite, 40 GHz and 12.5 GHz. (b) Data (solid) and inverted data (dot) pattern with BW = 12.5 GHz. The shaded region indicates possible waveform degradation region for time-multiplexing.

3.2 Effect of shaper resolution

The second system parameter analyzed is the pulse shaper resolution w_0, which we find to be one of the two critical parameters. For an optical grating based pulse shaper, as defined in Eq. (2b), pulse shaper resolution w_0 determines how faithfully the spatial mask function *M(x)* defined by the LCM pixel is transferred onto the effective filter function *H(ω)*. In static pulse shaping, maximizing shaper resolution (a smaller w_0) provides an *H(ω)* with higher resemblance to the mask function, hence better waveform fidelity. However, our findings show that for time-multiplexed line-by-line shaping, this rule may not hold.

We begin our analysis by modeling Eq. (1a), assuming only λ_a CW laser exists. We further assume that only two frequency comb lines, for example, lines at 0 and −10 GHz in Fig. 1(b), are selected by the pulse shaper. *H(ω)* is simulated using the parameters of our experiment: the physical width of each LCM pixel is 100 μm, while the spatial dispersion parameter, α = 3.18e-13 cm (rad/s)$^{-1}$, corresponds to 5 GHz frequency spread over 100 μm. Hence adjacent

#125479 - $15.00 USD Received 15 Mar 2010; revised 16 Apr 2010; accepted 19 Apr 2010; published 20 Apr 2010

comb lines separated by f_{rep} = 10 GHz are separated by two pixels (200 μm). Figure 3(a) shows when four LCM pixels (mask function in blue solid traces) are turned on to allow full transmission of two comb lines. This shaper setting yields a sinusoidal time-domain intensity waveform with 100 ps period. Resulting $H(\omega)$ (dots) for w_0 = 130 μm, w_0 = 85 μm and w_0 = 20 μm are shown respectively with the corresponding Gaussian intensity beams $G(x)$ as defined in Eq. (2b) (dashed traces). For a higher resolution (such as the w_0 = 20 μm case), the filter function indeed approaches the rectangular mask function, providing a sharp filter function to ensure clean line-by-line operation. As a comparison, in the w_0 = 130 μm case, the smoothened filter function clearly extends into the undesired adjacent comb lines. This gives rise to limited comb line suppression and leads to waveform degradation. The output comb lines fields $E_{out}(w)$ after the shaper is related to the input PMCW comb $E_{in}(w)$ through $E_{out}(\omega) = E_{in}(\omega)H(\omega)$. Figure 3(b) compares the spectral leakage effect for the three resolution values. The normalized output comb line fields are plotted along with the corresponding $H(\omega)$ trace (dots). To provide a quantitative comparison, for the w_0 = 130 μm case, the spectral leakages at the −20 and 10 GHz spectral locations (indicated by arrows) are 10.4% and 7.1%, respectively. For the w_0 = 85 μm case, due to a better resolution, the spectral leakages at the −20 and 10 GHz spectral locations are reduced to 1.4% and 1%, respectively. Up to this point, the findings are consistent to static line-by-line pulse shaping regime.

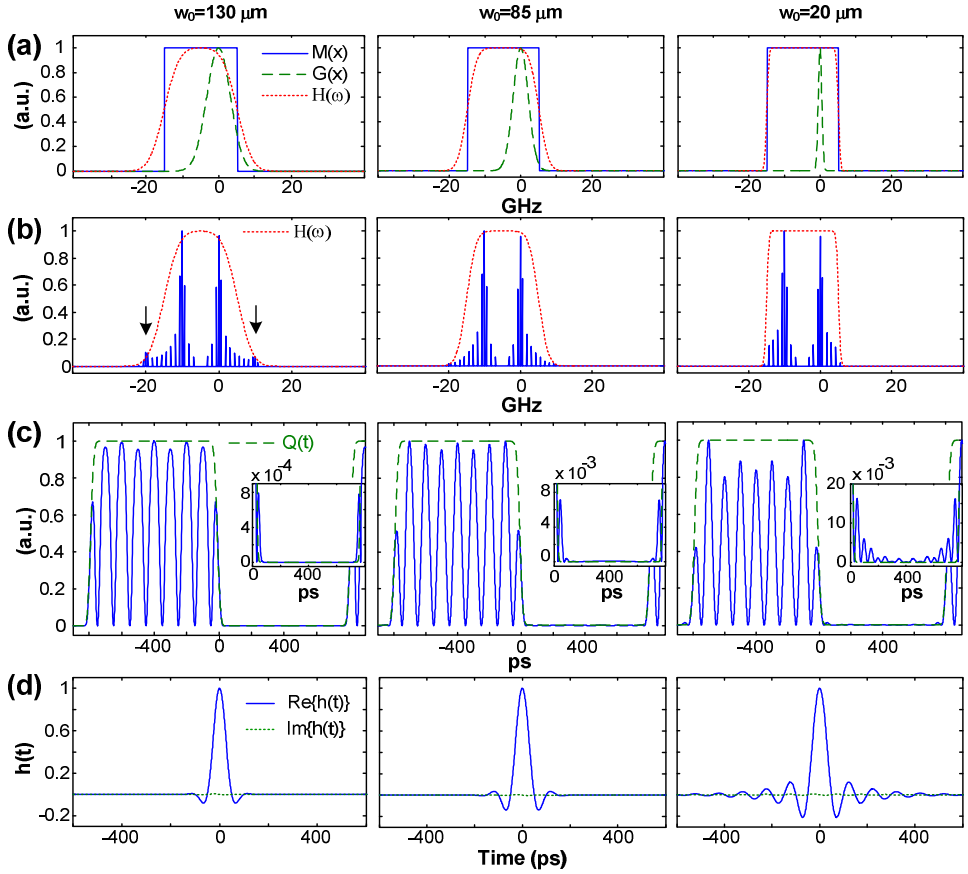

Fig. 3. (a) Mask function (M(x), solid), Gaussian intensity profile (G(x), dash) and the effective filter function (H(ω), dot) for w_0 = 130, 85 and 20 μm. (b) Output comb fields after the shaper illustrating spectral leakage. (c) Calculated intensity waveforms for various shaper resolution values with Q = [1111111100000000] and BW = 12.5 GHz. (d) Impulse response function of the corresponding pulse shaper.

#125479 - $15.00 USD Received 15 Mar 2010; revised 16 Apr 2010; accepted 19 Apr 2010; published 20 Apr 2010

We now illustrate the effect of shaper resolution on time-multiplexed waveforms. The time-domain waveforms (solids) for each resolution value are depicted in Fig. 3(c) along with the bandwidth limited Q = [1111111100000000] (dashes). For high shaper resolutions (w_0 = 85 and 20 μm), the shaped waveforms faithfully yield sinusoidal intensities; for a low shaper resolution (w_0 = 130 μm), the waveform deviate from the sinusoidal characteristics due to participation of the unsuppressed adjacent comb lines as described in the above paragraph. The longer pulse duration observed in the w_0 = 130 μm case is a special characteristic of the PMCW comb. The comb lines have intrinsic abrupt spectral phase jumps, as indicated in Fig. 1(b). Therefore a larger bandwidth in waveform generation without phase compensation actually yields longer pulses. This is different from pulse shaping performed on mode-locked lasers. Although giving better waveform fidelity, higher shaper resolution leads to larger intensity variations within the envelope of the generated sinusoidal intensity burst. This finding may be explained via Eq. (1a), where the time-domain output waveform is convolved with the shaper impulse response function. Figure 3(d) shows the time-domain impulse response functions for the three corresponding shaper resolutions. Here we have removed the linear temporal phase (equivalent to shifting the mask function centered at zero frequency) to facilitate comparison. As the shaper resolution increases, the rectangular-like effective filter function in the frequency-domain leads to the emergence of a sinc-function impulse response function. The longer wings of the sinc function lead to the observed larger intensity variations for higher shaper resolution, as well as intensity leakage into the OFF-bits, magnified on the insets in Fig. 3(c). This leakage will cause undesired waveform degradation when different parent waveforms are time-multiplexed, which will be discussed later. Interestingly, similar findings were reported in Ref [14]. in which the pulse shaping mask itself is assumed to be dynamically altered: excessive spectral resolution actually slows the rate at which waveforms may be changed. Therefore, in time-multiplexed line-by-line pulse shaping, an optimum resolution (of order w_0 = 85 μm as in our experimental shaper design) is desired to allow both spectral resolving power to ensure clean line-by-line shaping capability, while avoiding excessive pulse-to-pulse intensity variations. This may be viewed as an example of apodization, a concept well known in the signal and filter design literature [24,25]. The basic idea is to smooth transitions in the signal design (here the filter line shape) in order to suppress wings and sidelobes in the Fourier transform domain (here the impulse response function).

3.3 Effect of shaper extinction ratio

The third parameter under consideration is finite shaper power extinction ratio (η_{LCM}), which limits the waveform generation fidelity. Finite shaper extinction ratio arises due to the limited polarization extinction of the LCM, typically within the range of 20~30 dB. In our numerical model, finite η_{LCM} is incorporated into the mask function, where the zero-transmission state in the target shaper amplitude is restricted to a small nonzero value. Figures 4(a)–4(c) show the calculated time-multiplexed waveforms of single CW laser, two-line sinusoidal intensity waveform example, with η_{LCM} of infinite, 26 dB and 20 dB, respectively. Here we have reduced the pattern to an 8-bit Q = [11110000] to better discern waveform fidelity degradations. Pulse shaper resolution of w_0 = 85 μm is assumed to represent our experimental condition. These figures reveal that for a smaller shaper extinction ratio value, pulse-to-pulse ripple is increased in addition to the observed waveform deviation from the pure sinusoidal function. For example, in Fig. 4(c), sharp features within the pulse peaks are evident, indicating a larger spectral bandwidth (more comb lines) participate the waveform generation. This is a direct consequence of finite shaper extinction ratio as not being able to cleanly eliminate the undesired comb lines. In our physical system, our LCM power extinction ratio is nominally 26 dB.

#125479 - $15.00 USD Received 15 Mar 2010; revised 16 Apr 2010; accepted 19 Apr 2010; published 20 Apr 2010

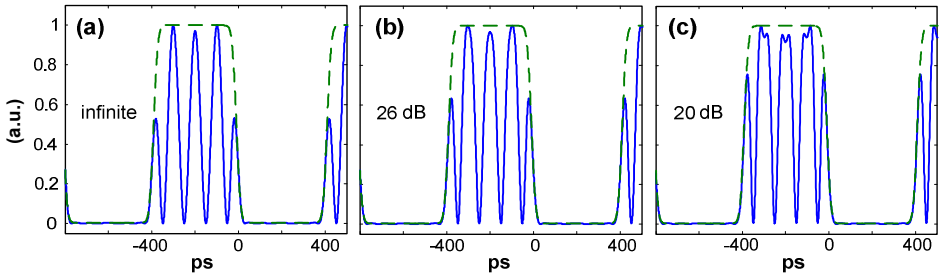

Fig. 4. Time multiplexed waveforms with shaper power extinction ratio η_{LCM} of (a) infinite, (b) 26 dB, and (c) 20 dB. Q = [11110000], w_0 = 85 μm and BW = 12.5 GHz are assumed.

3.4 Effect of intensity modulator extinction ratio

The impact of finite intensity modulator extinction ratio (η_{IM}) on time-multiplexed waveforms is now analyzed. Figures 5(a), 5(b) show the time-domain intensities of λ_a alone and λ_b alone, respectively, with η_{IM} of 13 dB. Here the λ_a laser waveform is the two-line 10 GHz sinusoid, while the λ_b laser waveform is a two-line 20 GHz sinusoid function obtained with a pulse shaping filter which allows lines at −10 and 10 GHz in Fig. 1(b) to pass (the pulse shaper is programmed to block the "0 GHz" comb line). Figures 5(c), 5(d) overlay the time-domain intensities of λ_a alone (dot), λ_b alone (dash) and the two laser waveforms time-multiplexed (solid) with η_{IM} of 13 dB and 20 dB, respectively. We have assumed w_0 = 85 μm, η_{LCM} = 26 dB and Q = [11110000]. From these two examples, we may conclude that the presence of finite intensity modulator extinction ratio only gives rise to fidelity degradation during the waveform transient regions (shaded). This degradation can be alleviated by using pattern generator and intensity modulator with higher electrical bandwidths, as noted in section 3.1.

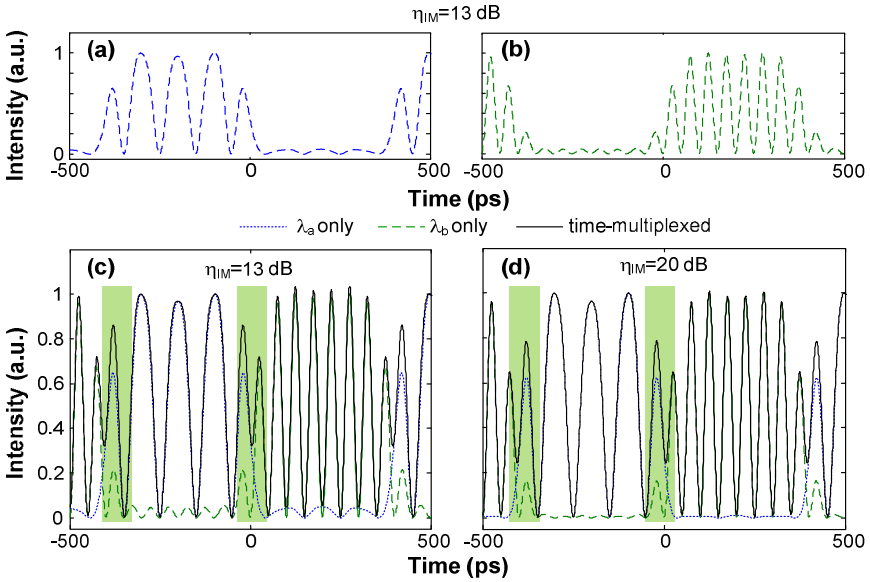

Fig. 5. Analysis on intensity modulator extinction ratio η_{IM} for time-multiplexed waveforms. Here Q = [11110000], w_0 = 85 μm, η_{LCM} = 26 dB are assumed. Intensities of (a) λ_a alone and (b) λ_b alone are shown, both with η_{IM} of 13 dB. (c) Intensities of λ_a alone (dot), λ_b alone (dash) and two waveforms time-multiplexed (solid) for η_{IM} of 13 dB. (d) Intensities of λ_a alone (dot), λ_b alone (dash) and two waveforms time-multiplexed (solid) for η_{IM} of 20 dB.

#125479 - $15.00 USD Received 15 Mar 2010; revised 16 Apr 2010; accepted 19 Apr 2010; published 20 Apr 2010

3.5 Combined effects

The above analysis has dealt with the system parameters independently. We now perform a combined analysis, in which we postulate three possible situations: ideal, realistic and worst case. The corresponding parameters for these three systems are listed in Table 1. In the following analysis, Q = [11110000]. The λ_a laser waveform generates the two-line 10 GHz sinusoid, while the λ_b laser generates the two-line 20 GHz sinusoidal function, similarly to that discussed in Fig. 5. Figure 6(a) shows the calculated time-domain intensities for the three systems without shaper phase control. The mask functions for the two waveforms are shown in Fig. 6(b). Similar to the results seen in Fig. 5, waveform distortion is minor for the λ_b laser waveform, but apparent for the 10-GHz λ_a laser waveform (within −400 to 0 ps). It is most evident to notice near time location −200 ps, the waveform degrades from the initial pure sinusoid (ideal: solid) to broadened pulse (real: dash) and then to doubly-peaked pulse (worst: dot).

Table 1. Parameter values for the three investigate systems.

System	Shaper resolution: w_0 (μm)	Intensity modulator extinction ratio: η_{IM} (dB)	Shaper extinction ratio: η_{LCM} (dB)	Intensity modulator BW value (GHz)
Ideal	85	60	50	40
Real	85	25	26	12.5
Worst	20	13	20	12.5

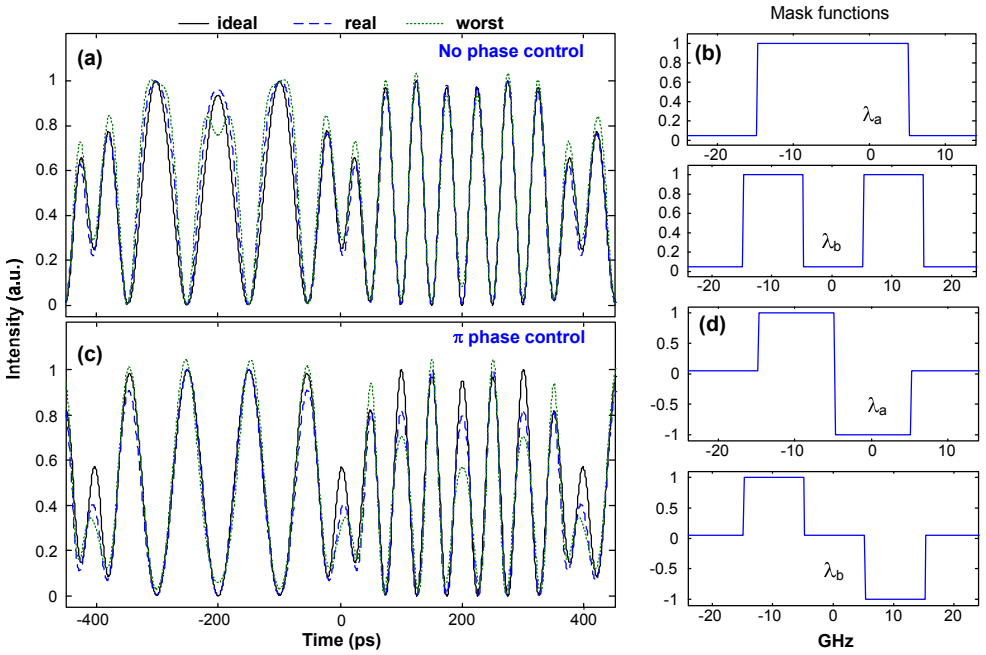

Fig. 6. Analysis on combined system effects. Time-domain intensities for ideal (solid), real (dash) and worst (dot) systems: (a) without phase control and (c) with one of each comb lines being applied a π phase. (b, d) Corresponding mask functions for the waveforms in cases (a, c), respectively.

Figure 6(c) shows the calculated time-domain intensities with shaper phase control. The mask functions for the two waveforms are shown in Fig. 6(d). One of the two comb lines from each laser are applied with a π spectral phase, resulting in both laser waveforms translated by half of their corresponding temporal periods. Interestingly, it is now the 20 GHz λ_b laser waveform (within 0 to 400 ps) enduring severe waveform distortion. As pulse shaper extinction ratio degrades, the λ_b laser waveform shows large pulse to pulse intensity variation as system parameters degrade. Apparently there is a residual 10 GHz spectral component

#125479 - $15.00 USD Received 15 Mar 2010; revised 16 Apr 2010; accepted 19 Apr 2010; published 20 Apr 2010

contributing to this effect, coming predominantly from finite shaper extinction ratio. To understand the origin of this phenomenon, Fig. 7(a) shows the schematics of the λ_b output comb lines (denoted by arrows) for as the discussions made in Fig. 6(b) while Fig. 7(b) for phase control as in Fig. 6(d). For clarity, the additional sidebands under the presence of data modulation are ignored. Due to finite shaper extinction, the unsuppressed comb lines at (–20, 0, 20) GHz are denoted using shorter arrow to indicate weaker amplitudes. We may acquire the knowledge of the overall 10 GHz strength by the beatings of every two adjacent comb lines, as indicated within the figures. Due to symmetry of the comb, b1 denotes the beating strength between lines at (–20, –10) and (10, 20) GHz, while b2 denotes the beating strength between lines at (–10, 0) and (0, 10) GHz. A negative sign incurs whenever the two comb lines are π out of phase. For the case in Fig. 7(a), the sum of all the 10 GHz beatings comes to zero, and therefore a pure 20 GHz sinusoidal function as seen in Fig. 6(a). For the case in Fig. 7(b), due to the π phase control to the 10-GHz line, the sum of all the 10 GHz beatings is nonzero, leading to the large intensity variation from one peak to the next seen in Fig. 6(c). These two examples show that our current (real) system parameters can be improved in the future by incorporating LCM with higher extinction ratios.

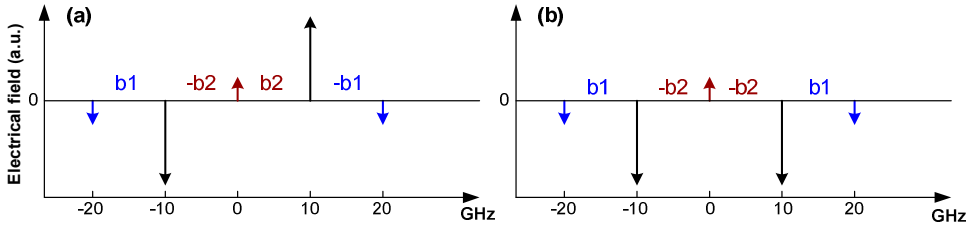

Fig. 7. Schematic of the λ_b shaped output comb lines for (a) phase control as in Fig. 6(a), 6(b) and (b) for phase control as in Fig. 6(c), 6(d). For clarity, the additional sidebands due to data modulation are ignored. The arrows denote the comb lines while the lengths of the arrows represent the line field strengths.

4. Fitting to experiment

We have now acquired some understanding of how various factors affect the time-multiplexed waveform generation process. We now present two examples of experimental data [15,16] compared to simulation results. In the experiments the time-multiplexed waveforms are sent to an optical detector with 60 GHz electrical bandwidth and characterized both in the time-domain and in the electrical frequency-domain. The time-domain intensities are measured using a sampling scope with 50 GHz bandwidth, while the RF power spectra are obtained via an electrical spectrum analyzer (ESA: Agilent 8565EC with 30 Hz to 50 GHz). ESA resolution bandwidth of 100 kHz is used to acquire the electrical power spectra.

For the two experimental cases shown in Fig. 8, data pattern of Q = [1111111100000000] is used. Our data fitting process follows our analysis: we begin by using only λ_a laser, and only two adjacent comb lines are selected. Figure 8(a) shows the experimental (solid) and calculated (dots) time domain intensity traces Fig. 8(b) shows the corresponding experimental (solids) and calculated (circles) RF power spectra. Through our fitting process, we find that different system parameter value can be extracted from different parts of the experimental data, and the RF power spectra are necessary to acquire complete understanding related to all system parameters. Our finding shows that the shaper resolution, intensity modulator electrical bandwidth and the intensity modulator extinction ratio values can be obtained from the waveform intensity trace, while the shaper extinction ratio value is better obtained from the RF power spectra.

We now explain how the system parameters are determined step-by-step: The shaper resolution has been determined as the most critical parameter and should be acquired first. A rough estimate for the shaper resolution value of w_0 ~80 μm have been obtained

#125479 - $15.00 USD Received 15 Mar 2010; revised 16 Apr 2010; accepted 19 Apr 2010; published 20 Apr 2010

experimentally via fitting the effective shaper filter function by sweeping a tunable CW laser, as reported in Ref [17]. Using the waveform intensity trace in Fig. 8(a), precise w_0 value of 85 μm is first obtained. Intensity modulator electrical bandwidth of BW = 12.5 GHz is then acquired through fitting the two waveform transition edge profiles, indicated by the two dotted boxes. Intensity modulator extinction ratio of 25 dB is obtained by fitting the OFF-bits intensity trace, indicated by the dashed circle.

While the previous three parameters can be extracted through fitting the time-domain intensity trace, minor variation in shaper extinction ratio is a not as obvious. At this point the experimental RF power spectrum can then be used to deduce the exact shaper extinction ratio. Finite extinction yields unsuppressed comb lines, and gives rise to higher harmonic peaks of the phase modulation frequency. Shaper extinction ratio of 26 dB is deduced by focusing on the fit of the unsuppressed 20 GHz peaks highlighted in the dashed circle.

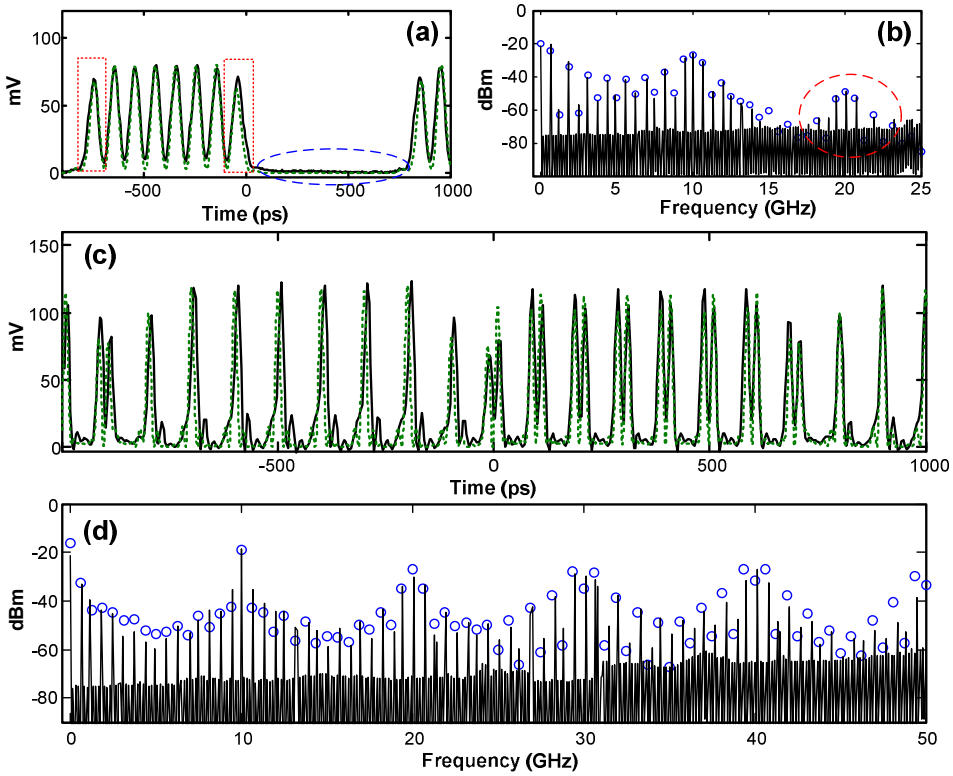

Fig. 8. Fittings to experimental data with Q = [1111111100000000]. Time-domain intensity (a) and the electrical current power spectrum (b) for a single CW laser. Time-domain intensity (c) and the electrical current power spectrum (d) for rapidly switched transform-limited pulse and odd pulse. Data are shown in solid lines while calculations are shown in dotted lines or circles. In (b,d), ESA resolution bandwidth is 100 kHz.

The resulting fits in Fig. 8(a), 8(b) indicate our numerical model is well capable of calculating the detailed time-domain waveform profile as well as the RF power spectrum. In the time-domain traces, excellent agreements between experimental data and our calculation in terms of periodicity, relative magnitudes of the eight peaks within the ON-bits have been obtained. It is also noteworthy that the system parameters extracted through the fitting process corroborate our prior understanding for static pulse shapers (such as shaper resolution and extinction ratio values) as well as vendor specifications (such as modulator and pattern generator bandwidth).

Using the four system parameter values deduced from the single laser case, we now perform a calculation for the dual-laser case. In Figs. 8(c), 8(d) both CW lasers and all seven

#125479 - $15.00 USD Received 15 Mar 2010; revised 16 Apr 2010; accepted 19 Apr 2010; published 20 Apr 2010

comb lines as shown in Fig. 1(b) from the resulting two PMCW combs are used. The pulse shaper is programmed so that transform-limited pulses (λ_a comb) and doublet pulses (λ_b comb with a π phase jump across half of the spectrum) are rapidly time-multiplexed. In Fig. 8(c), 8(d), time-multiplexing of seven-comb-line waveforms generates electrical spectrum spanning the entire 0-50 GHz ESA bandwidth, with a modulated envelope peaking at 10 GHz and its harmonics. Note that not only the time-domain waveforms are truthfully fitted, but also the RF power spectra are in close quantitative agreement. From these examples, the validity of our numerical model is well justified. We attribute the slight deviations in the waveform ripples and satellite pulses observed in Fig. 8(c) to the fact that finite electrical bandwidth of the photo-detector, sampling scope and the ESA are not yet considered. Nevertheless, the current model is sufficient to aid in designing complex arbitrary microwave waveforms and spectral synthesis.

5. Summary and discussion

In summary, a numerical model for time-multiplexed line-by-line shaping system is developed. Effects of system parameters on time-multiplexed waveforms are analyzed numerically. Two experimental rapidly switched time-domain waveforms and the corresponding electrical power spectra were fitted using our numerical results with excellent agreement. The validity of the model should allow added functionality for high-speed optical arbitrary waveform generations. A possible future direction is to include the effects of finite electrical bandwidth of the photo-detector, sampling scope and the electrical spectrum analyzer. Another potential future development target is to compensate for the output distortions due to the non-ideal shaping parameters. For instance, fine-tuning of the effective line-by-line filter function from the nominal specification could be a solution to further approximate to the target the outputs affected by non-idealities. One may also envision flexible millimeter-wave spectral synthesis with substantially higher complexity and covering from the radio-frequency range all the way into the terahertz regime using the same approach.

Acknowledgement

Chen-Bin Huang was supported by the National Science Council of Taiwan under contract NSC 97-2112-M-007-025-MY3. Andrew M. Weiner was supported in part by the Naval Postgraduate School under grant N00244-09-1-0068 under the National Security Science and Engineering Faculty Fellowship program.

#125479 - $15.00 USD Received 15 Mar 2010; revised 16 Apr 2010; accepted 19 Apr 2010; published 20 Apr 2010